

# Tectonics

## RESEARCH ARTICLE

10.1029/2019TC005941

### Key Points:

- Curvature of the Fars Arc, eastern Zagros, is proposed to be achieved by vertical axis rotations of fault bounded blocks
- Regional rotations determined from GPS data are the opposite sense to “bookshelf” model predictions
- Intersection of active folds of different orientations produces domal fold interference patterns, without separate deformation phases

### Correspondence to:

M. B. Allen,  
m.b.allen@durham.ac.uk

### Citation:

Edey, A., Allen, M. B., & Nilfouroushan, F. (2020). Kinematic variation within the Fars Arc, eastern Zagros, and the development of fold-and-thrust belt curvature. *Tectonics*, 39, e2019TC005941. <https://doi.org/10.1029/2019TC005941>

Received 22 OCT 2019

Accepted 26 JUN 2020

Accepted article online 30 JUN 2020

## Kinematic Variation Within the Fars Arc, Eastern Zagros, and the Development of Fold-and-Thrust Belt Curvature

A. Edey<sup>1,2</sup>, M. B. Allen<sup>1</sup> , and F. Nilfouroushan<sup>3,4</sup> 

<sup>1</sup>Department of Earth Sciences, University of Durham, Durham, UK, <sup>2</sup>Office for Nuclear Regulation, Liverpool, UK, <sup>3</sup>Department of Computer and Geospatial Sciences, University of Gävle, Gävle, Sweden, <sup>4</sup>Department of Geodetic Infrastructure, Geodata Division, Lantmäteriet, Gävle, Sweden

**Abstract** We analyze deformation of the Fars Arc in the eastern Zagros, Iran, including earthquake slip vectors, GPS velocities, paleomagnetism data, and fold orientations, to understand how this fold-and-thrust belt works and so better understand the generic issue of fold-and-thrust belt curvature. The Fars Arc is curved, convex southward. GPS-derived rotation rates are  $\leq 0.5^\circ \text{ Myr}^{-1}$ : Rotation is clockwise west of  $53^\circ \text{E}$  and counterclockwise to the east. These rotation senses are opposite to previous predictions of passive “bookshelf” models for strike-slip faults during north-south convergence. West of  $53^\circ \text{E}$ , average GPS vectors, thrust earthquake slip vectors, strain axes derived from GPS data, and orthogonal directions to fold trends are all aligned, toward  $\sim 218^\circ$ . East of this meridian, the average GPS vector is toward  $208^\circ$ , but the averages of the other data sets are distinctly different, all toward  $\sim 190^\circ$ . We propose that fault blocks in eastern Fars, each  $\sim 20\text{--}40$  km long, rotate predominantly counterclockwise, whereas in western Fars, the regional clockwise rotation takes place mainly on the array of active right-lateral faults in this area. Thus, localized block faulting and rotations accumulate to produce the overall strain and regional curvature. Active folds of different orientations in eastern Fars intersect to produce domal interference patterns, without involving separate deformation phases, indicating that fold interference patterns should not be interpreted in terms of changing stress orientations unless there is clear evidence. Fars Arc curvature is best explained by deformation being restricted at tectonic boundaries at its eastern and western margins, with significant gravitational spreading.

## 1. Introduction

This paper addresses the kinematics of the fold-and-thrust belt in the Fars Arc region of the eastern Zagros, and particularly the mechanism for its curvature. The Fars Arc shares this property with numerous active and inactive fold-and-thrust belts worldwide, such as the Himalaya and the Suleiman Range in Pakistan, but the origins of such curvature have long been debated and are still contentious (e.g., Macedo & Marshak, 1999; Copley, 2012). Hindle and Burkhard (1999) summarized two end-member kinematic schemes for the formation of curved fold-and-thrust belts during the original phase of deformation (as opposed to later bending of an originally straight belt): These are “Piedmont glacier,” with divergent transport direction during deformation, and “Primary arcs,” with uniform transport direction but variable strain rate during deformation (Figure 1).

The Zagros is tectonically active (Figure 2) and so a useful example for comparison with inactive belts worldwide. Additionally, the results bear on several other aspects of Zagros evolution that are debated: (1) whether or not the Zagros has been affected by two distinct episodes of deformation, with a transition from thin-skinned to thick-skinned tectonic style (Leturmy et al., 2010; Molinaro et al., 2005); (2) the interactions of vertical axis rotations, strike-slip faulting, and thrust faulting (Hessami et al., 2001; Talebian & Jackson, 2004); and (3) the role of the Hormuz Series salt in controlling the style and distribution of deformation (Authemayou et al., 2006; Koyi et al., 2016; Talbot & Alavi, 1996).

In this study, we analyze earthquake slip vectors, fold patterns, published GPS data, and available paleomagnetic data from the Zagros fold-and-thrust belt, with the aim of understanding the deformation of the eastern part of the region, the Fars Arc. The rationale is that combination and comparison of these data sets give insights into tectonic processes that cannot be achieved in ancient, inactive orogens where such approaches are not available. In particular, active regions where there are mismatches between the GPS and earthquake slip vectors strongly imply some form of strain partitioning and/or vertical axis rotations have taken place

©2020. The Authors.

This is an open access article under the terms of the Creative Commons Attribution License, which permits use, distribution and reproduction in any medium, provided the original work is properly cited.

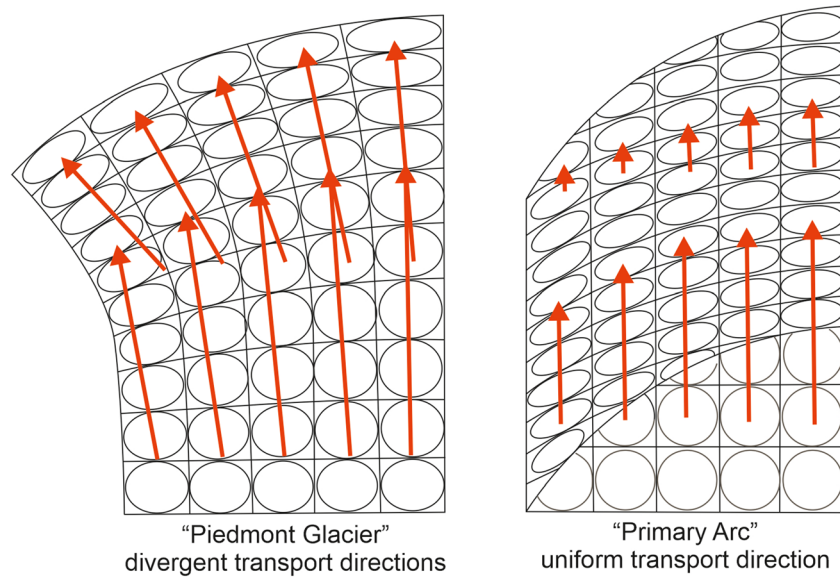


**Figure 1.** End-member models of fold-and-thrust belt curvature, where curvature develops during the original period of deformation. Red arrows indicate convergence velocities across the system, analogous to a GPS-derived velocity field. Ellipses are schematic strain markers. From Hindle and Burkhard (1999).

(e.g., Bayasgalan et al., 2005) and permit understanding of the processes involved. We also analyze the local orientations of folds in the light of the slip vector data, to understand processes that might cause fold interference patterns in eastern Fars.

## 2. Regional Geology

An impetus for studying the Zagros is that it is one of the most seismically active fold-and-thrust belts on Earth (Hatzfeld et al., 2010; Nissen et al., 2011; Oveisi et al., 2009; Talebian & Jackson, 2004) and is a major part of the Alpine-Himalayan orogenic system (Agard et al., 2011; Hatzfeld & Molnar, 2010), and the Arabia-Eurasia collision in particular. As such, the region is a superb area to study continental tectonic processes, while the natural hazards represented by earthquakes pose significant challenges to society.

The NW-SE-trending Zagros fold-and-thrust belt extends for about 2,000 km, from eastern Turkey, through northern Iraq (Kurdistan) and southern Iran, to the Makran subduction zone at the Iran-Pakistan borderlands (Mouthereau, 2011). The Zagros formed as the Neo-Tethys Ocean closed and Arabia and Eurasia collided. The timing of the initial collision is debated and estimates range from the Late Cretaceous to the Pliocene, although most studies put it in the range of 20–35 Ma (e.g., Allen & Armstrong, 2008; Barber et al., 2018; Koshnaw et al., 2019; McQuarrie & van Hinsbergen, 2013).

Collision is still strongly active, demonstrated by the abundant seismicity across southwest Asia (Figure 2) and the high topography of the Zagros, Turkish-Iranian Plateau, and ranges on the northern side of the collision zone such as the Alborz. GPS-derived convergence rates increase eastward from 16–26 mm yr<sup>-1</sup> across the collision zone and are ~20 mm yr<sup>-1</sup> at the longitude of Tehran, roughly 51°E (Vernant et al., 2004). There is a change in convergence orientation across the collision zone; convergence in the west is toward the NNW, and in the east toward the NNE (Figure 2). The Arabia-Eurasia pole of rotation lies in the eastern Mediterranean region. Strain is not evenly distributed across the collision zone, shown by the uneven distribution of seismicity; active thrusting is concentrated at the margins of the system, such as the Zagros and Alborz fold-and-thrust belts at the southern and northern sides of the Iranian Plateau (Jackson, 2001). Overall convergence rates may have slowed since ~5 Ma, perhaps because the elevated topography of the thickened collision zone resisted shortening (Austermann & Iaffaldano, 2013), but there does not appear to have been a major change in plate convergence azimuth through the late Cenozoic (McQuarrie et al., 2003). Therefore, there is no known plate-scale reorganization to explain any discrepancies between geodetic data and longer-term markers of strain.

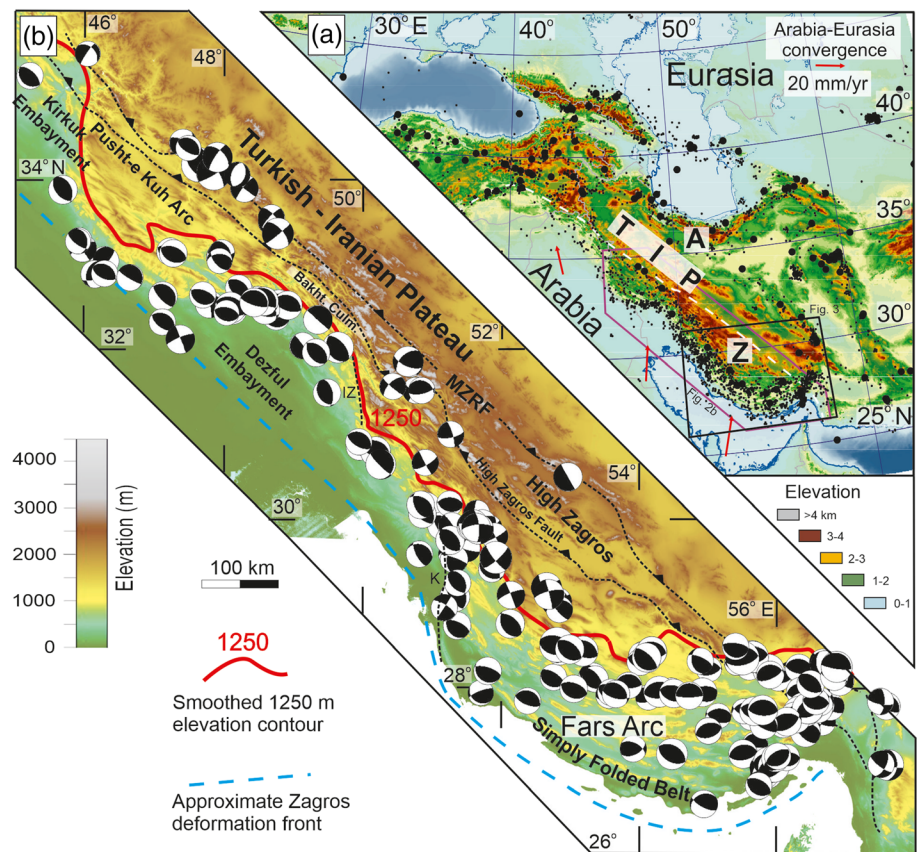


**Figure 2.** (a) Regional topography and seismicity of the Arabia-Eurasia collision. Large dots are epicenters of earthquakes of  $M > 6$  from 1900 to 2000 (Jackson, 2001), small dots are epicenters from the EHB catalog 1964–1999,  $M > 5$ . Red arrows show GPS-derived velocity with respect to Eurasia from Sella et al. (2002). A, Alborz; TIP, Turkish-Iranian Plateau; Z, Zagros. White dashed line indicates the original Arabia-Eurasia suture. (b) Seismicity of the Zagros: Focal mechanisms reported in Nissen et al. (2011) and references therein. MZRF, Main Zagros Reverse Fault (Zagros suture); IZ, Izeh Fault; K, Kazerun Fault. Modified from Allen et al. (2013).

The Main Zagros Reverse Fault (Figure 2) is the position of the original Arabia-Eurasia suture (Agard et al., 2011) and is located at the northeast side of the Zagros: The Zagros fold-and-thrust belt is developed over what was the passive continental margin of the Arabian Plate before collision. The Main Zagros Reverse Fault trends northwest-southeast along the length of the Zagros (Figure 3). The Zagros can be divided into two main zones across strike. To the northeast is an ~100 km wide zone called the High Zagros, which averages 1.5–2 km in elevation, with some peaks exceeding 4,000 m (Figure 2). To the southwest is the 100–200 km wide Simply Folded Belt (SFB), which rises from sea level in the southwest to 1.5 km in the northeast (Nissen et al., 2011).

The structure and geomorphology of the Zagros vary along strike (Berberian, 1995; Obaid & Allen, 2019). Folds (and underlying thrusts) near the northern tip of the Arabian Plate trend roughly east-west, but this trend swings to a northwest-southeast orientation that is maintained along the majority of the length of the range. The deformation front is roughly linear and subparallel to the suture as far east as 51°E, but there are two main areas of subdued relief, topography and exhumation, known as the Kirkuk and Dezful embayments (Figure 2). These regions are separated by the Pusht-e Kuh Arc. The eastern margin of the Dezful Embayment is somewhat gradational and defined by north-south-trending right-lateral faults such as the Izeh Fault and the Kazerun Fault (Sherkati et al., 2006).

The Fars Arc is the ~700 km long segment of the Zagros from the east of the Kazerun Fault to the eastern limit of the range (Figure 3), where there is a transition into the Makran accretionary complex (Bayer et al., 2006; Mouthereau et al., 2007). It is arcuate in plan view, in contrast with the more linear segments

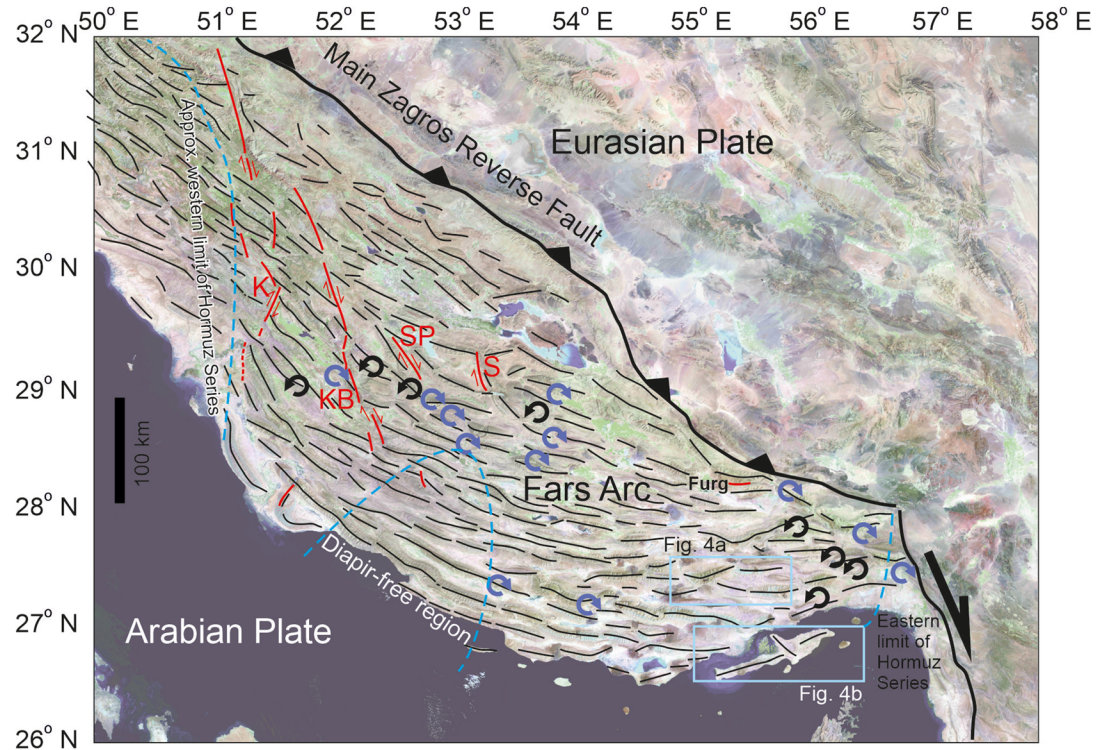


**Figure 3.** Eastern Zagros (Fars Arc) anticline trends superimposed on a MrSID Landsat 7 mosaic, showing the broad change in fold orientation across this part of the Zagros fold-and-thrust belt. Red lines are emergent fault traces within the Zagros. K, Kazerun; KB, Karih Bas; SP, Sabz Pushan; S, Sarvestan. Blue dashed lines show the extent of the Hormuz Series salt, southwest of the Main Zagros Reverse Fault (Kent, 1979), based on the distribution of diapirs; the diapir-free region in the center of the Fars Arc does not appear to affect fold style. Circular arrows are paleomagnetically derived rotation senses, shaded by rotation sense, from Bakhtari et al. (1998), Smith et al. (2005), and Aubourg et al. (2008, 2010).

to the northwest. Folds trend NW-SE in the west in the Fars Arc, meaning that at this side of the Fars Arc, there is no contrast to regions further west. Fold trends change eastward, to ENE-WSW in the east of the region (Figure 3). The Fars Arc is also characterized by a deformation front that lies further south than the continuation of the line of the linear deformation front to the northwest (Figure 2).

The western side of the Fars Arc region is marked by the Kazerun Fault (Figure 3). Right-lateral offset has been estimated to be as high as 160 km (Berberian, 1995; Hessami et al., 2001), but these estimates were based on the distance between geomorphic steps that were never contiguous. Analysis of bedrock displacement gives offsets in the order of only ~8 km (Authemayou et al., 2006). East of the Kazerun Fault, the Karih Bas, Sabz Pushan, and Sarvestan faults distribute right-lateral slip across a broad area of the western Fars region (Figure 3; Tavakoli et al., 2008; Sarkarinejad et al., 2018). Bedrock offsets of these faults are in the same range as the Kazerun Fault, and from ~7–13 km (Authemayou et al., 2006). Fault segments are typically tens of km long, discontinuous, and have variable orientations. These right-lateral faults in western Fars are the only seismically active faults that are also exposed (Nissen et al., 2011), with the rare exception of the  $M_w$  6.4, 6 November 1990 Furg earthquake surface rupture, near the eastern Main Zagros Reverse Fault (Walker et al., 2005) (Figure 3).

The ~1 km thick Precambrian-Cambrian Hormuz Series salt is present across large parts of the Zagros (Jahani et al., 2007; Kent, 1979). It appears at the surface because of diapirs that occur across the Fars Arc. There is an area in the central part of Fars where there are no diapirs (Figure 3). The Hormuz Series salt also appears at the base of thrust sheets in the High Zagros, northeast of the Dezful Embayment. The subsurface distribution is more speculative. Stratigraphy indicates that the salt diapirs partially predate the Arabia-Eurasia collision (Kent, 1979). The Hormuz Series salt has long been used to infer a detachment at the base of the Zagros stratigraphy (e.g., Bahroudi & Koyi, 2003; Falcon, 1974; McQuarrie, 2004).

However, the seismicity record clearly indicates the presence of significant thrusting in the basement (Nissen et al., 2011; Talebian & Jackson, 2004). Basement and cover deformation must be coupled in some way (Allen et al., 2013; Lacombe et al., 2011; Nilfouroushan et al., 2013), notwithstanding the ability of the Hormuz Series salt to impede smaller earthquakes from propagating through it (Nissen et al., 2011). Talebian and Jackson (2004) noted that there are only a few thrust earthquakes in the High Zagros and those that are recorded are in the southeastern region, where elevations are lower. The limit for seismogenically significant ( $M_w > 5$ ) thrusting is close to the regional 1,250 m elevation contour (Nissen et al., 2011).

Several estimates of shortening across the Fars region have been made, with estimates typically in the range of ~60–80 km (e.g., Allen et al., 2013; McQuarrie, 2004; Mouthereau, 2011). Surface shortening is accommodated by trains of parallel anticlines and synclines. The mostly symmetric folds have kilometer-scale amplitudes and wavelengths of ~10–20 km; these are examples of the famous whaleback anticlines that characterize the Zagros. Low-angle thrust faults are rare in the SFB, but blind thrust faulting is common and dominates the seismicity in the region (Nissen et al., 2011).

Estimated active shortening rates across the Zagros vary from  $5 \pm 3 \text{ mm yr}^{-1}$  (NW) to  $9 \pm 3 \text{ mm yr}^{-1}$  (SE) (Hessami et al., 2006; Vernant et al., 2004; Walpersdorf et al., 2006), consistent with the greatest amount of finite shortening occurring across the regions in the southeast (e.g., Mouthereau, 2011). The right-lateral strike-slip faults within western Fars have a slip rate of  $\sim 4 \text{ mm yr}^{-1}$  and appear to have propagated southward through the Pliocene-Quaternary (Tavakoli et al., 2008). Strain partitioning occurs in the northwest of the Zagros fold-and-thrust belt (e.g., Raeesi et al., 2017; Talebian & Jackson, 2004; Zarifi et al., 2014), based on analysis of earthquake focal mechanisms and geodetic measurements: Northeast-southwest shortening across the northwest Zagros is accompanied by range-parallel, right-lateral strike-slip faulting along the Main Recent Fault, which roughly follows the trace of the Main Zagros Reverse Fault in this region.

Paleomagnetic studies of the Fars Arc have detected vertical axis rotations during the late Cenozoic deformation (Aubourg et al., 2008, 2010; Bakhtari et al., 1998; Smith et al., 2005). These rotations are broadly clockwise in the western part of the Fars Arc and counterclockwise in the east, although there is considerable local variation (Figure 3). Total amounts of rotation in either direction are typically  $\leq 25^\circ$ . Deriving long-term rotation rates requires accurate determinations for the duration of rotation, which is not constrained. Nor is the age of each unit clear; nonmarine stratigraphy across the Zagros is diachronous (Fakhari et al., 2008; Ruh et al., 2014). These total rotations and loosely constrained ages indicate that long-term rotation rates on the order of at least  $1\text{--}2^\circ \text{ Myr}^{-1}$  are plausible for the last 5–10 million years.

### 3. Data and Methods

The rationale of this paper is to examine structural, geomorphic, seismicity, and geodetic data in one study, to understand better the causes of the distinct fold-and-thrust belt curvature of the Fars Arc. This section sets out the sources of each data set and the processing applied; section 4 sets out the results. Data fall into two categories: those types that represent neotectonic, recent, deformation (geodetic and seismicity data) and data that represent long-term strain (fold axial traces and published paleomagnetic data).

Folds are well exposed and preserved across the Fars region, partly because of the tectonic activity and semi-arid climate. Fold preservation is enhanced by a strong mechanical stratigraphy in Tertiary and Cretaceous carbonate formations: These units resist erosion and so preserve complete anticlines at the surface (Figures 2 and 3). Figure 3 is a summary map of anticline axial traces and emergent faults, drawn from Landsat satellite imagery (presented in the form of MrSID mosaics), complemented by analysis of 1:1M and 1:200,000 NIOC and Geological Survey maps of the region, and the Shuttle Radar Topography Mission (SRTM) 90 m data set. We use these sources to measure anticline fold orientations across the Fars Arc ( $n = 301$ ) and to interpret specific examples of composite folds (Figure 4).

Earthquake focal mechanism data for the Fars region are from Talebian and Jackson (2004), Nissen et al. (2011), and, for 2011–2014, from the Global CMT catalog (<https://www.globalcmt.org/>) (Dziewonski et al., 1981; Ekström et al., 2012) (Figure 5). Reliability was determined from double-couple values (see Jackson et al., 2002 for discussion of this approach), with the data displayed in Figure 5 plotted according to whether double-couple values are  $< 70\%$  or  $\geq 70\%$ . The latter category contains 53 events, and these data

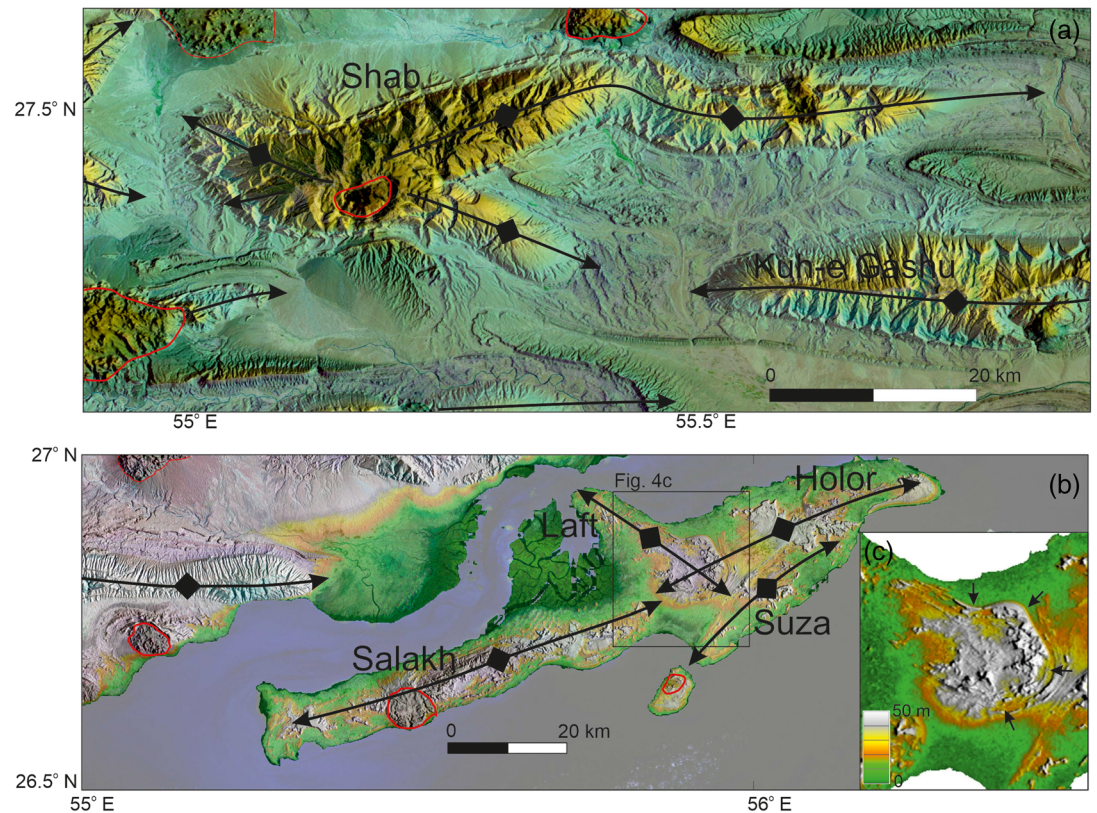


**Figure 4.** Examples of synchronous, mutually cross-cutting active anticlines in the Fars Arc, illustrating how domal fold interference patterns can occur without separate episodes of deformation. Images are MrSID Landsat 7 mosaics draped over SRTM 90 m topography. Red outlines highlight Hormuz salt diapirs. Lines with black diamonds are anticline axial traces, with plunge arrows marked at fold terminations. (a) Shab anticline; the exposed core of the fold consists mainly of carbonates of the Eocene-Oligocene Asmari-Jahrom Formation (b) Qeshm island anticlines. Folded strata are predominantly from the Mishan and Agha Jari formations (Miocene and Pliocene) (c) close-up of domal topography and outcrop patterns at the intersection of the Laft and Holor anticlines. Black arrows highlight domal folding of a horizon in the Upper Miocene(?) Agha Jari Formation. Locations shown on Figure 3.

are used to construct the plot of earthquake slip vector azimuths shown in Figure 6. These slip vectors are presented in thrust and strike-slip categories, with thrust motion shown toward the south (Arabian Plate) and strike-slip toward the east. For the better constrained events, uncertainties of strike and hence slip vector azimuth are in the order of  $\pm 15\text{--}20^\circ$  (Jackson et al., 2002). Errors in the best teleseismically recorded epicenters are  $\sim 10\text{--}15$  km (Engdahl et al., 2006), making it impractical to associate individual earthquakes with specific structures.

For comparison with the slip vectors, GPS velocity data are plotted on Figure 7. Whereas earthquake slip vectors show the relative motion between the blocks on either side of the fault, GPS vectors show the motion of the measured point with respect to the chosen reference frame. We transformed the Eurasian-fixed GPS velocities (Khorrami et al., 2019) using the rotation pole between Eurasia and Arabia in the ITRF2008 reference frame (Altamimi et al., 2012) to illustrate the GPS velocities relative to the Arabian Plate (Figure 7).

We computed the geodetic rotation rates on a  $75\text{ km} \times 75\text{ km}$  rectangular grid using the SSPX program (Cardozo & Allmendinger, 2009). Using the GPS horizontal velocities reported by Khorrami et al. (2019) and similar to previous studies (Allmendinger et al., 2007; Raeesi et al., 2017; Zarifi et al., 2014), we applied the Grid-Distance Neighbor method which uses weighted least squared adjustment where each station is weighted by its distance to the center of the cell. In the calculations, we used  $\alpha = 150$  km, where  $\alpha$  is a constant that specifies how the closeness of the stations to the center of the cell influences the strain solution. The obtained rotation rates (Figure 8) show the block rotation rates about the vertical axis, which are compared later with seismicity and paleomagnetic studies.

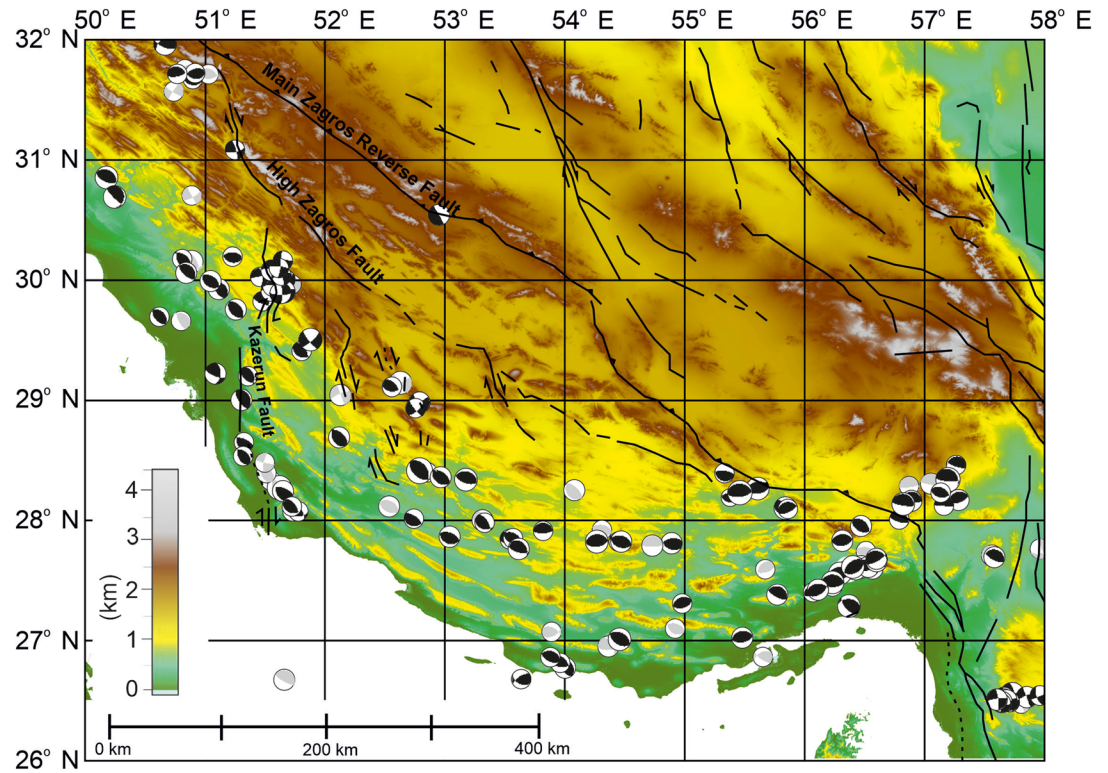


**Figure 5.** Eastern Zagros topography and earthquake focal mechanisms, derived from Nissen et al. (2011) and the Global CMT catalog. Higher quality solutions are in black (double couple  $\geq 70\%$ ). Thrust earthquakes are concentrated at lower elevations, below the regional 1,250 m elevation contour.

We also plot the axes for the maximum geodetic strain rate within the Zagros (Figure 9), derived from GPS data by Raeesi et al. (2017), for comparison with the other strain data in this study.

#### 4. Results

The summary structural map in Figure 3 is similar to previous publications for the Zagros (e.g., Berberian, 1995; Blanc et al., 2003; Mouthereau et al., 2012), which is not surprising given the obvious trends of the exposed folds. Changes in fold orientation across the region from NW-SE to ENE-WSW pick out the arcuate nature of the Fars Arc. Figure 3 emphasizes this broad variation in the fold orientation across the Fars Arc. West of the Kazerun Fault, folds are consistently aligned NW-SE, but east of this structure, more east-west folds and some ENE-WSW trends occur, becoming predominant to the east of  $\sim 53^\circ\text{E}$  (Figure 3). Geodetic strain axes are almost orthogonal to the fold trends (Figure 9) and their azimuths change from east to west as folds' trends change accordingly. The average direction of the orthogonals to the fold trends, west of  $53^\circ\text{E}$ , is  $218^\circ \pm 25^\circ$ ; east of  $53^\circ\text{E}$ , the average is  $189^\circ \pm 20^\circ$ . These data are not weighted for fold length. Kinematic data are summarized in Table 1.

The longer folds (80–100 km length) are composites of shorter segments, each typically on the length scale of 20–40 km (Ramsey et al., 2008). Some folds change orientation across the right-lateral strike-slip faults in the western Fars (e.g., Aubourg et al., 2008; Blanc et al., 2003), with counterclockwise rotations indicated by the more east-west orientations of folds to the east of the strike-slip faults.

There are mutual cross-cutting relationships in the eastern Fars Arc between folds with different orientations (Figures 4a and 4b). Different orientations of folds are similar in terms of their size, exposure level, amplitude and wavelength, and topographic relief (Figure 4). The Shab Anticline (Kuh-e Shu) has a main segment  $\sim 40$  km long, trending ENE (Figure 4a), with Asmari-Jahrom Formation carbonates exposed along the greater part of its length (Leturmy et al., 2010). The eastern end of this segment curves in a clockwise direction, and the remaining portion of the fold trends more east-west. The western part of the fold is

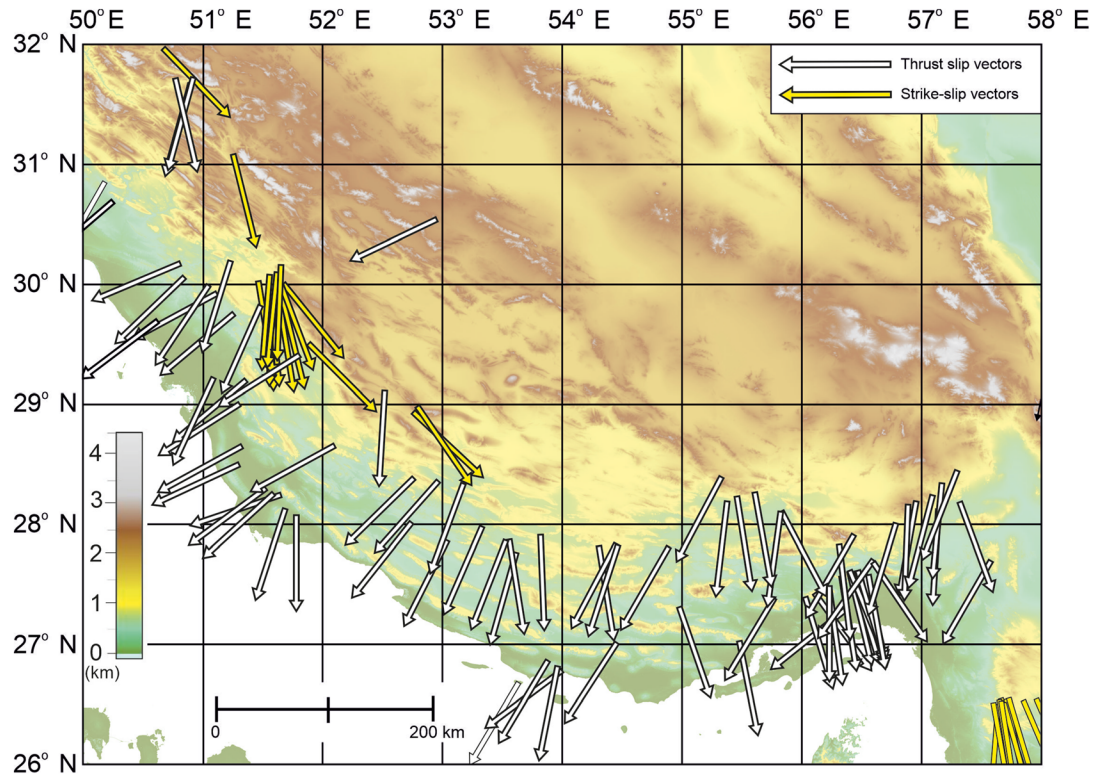


**Figure 6.** Earthquake slip vector azimuths from data in Figure 5. Average orientations are summarized in Table 1, for the regions west and east of 53°E, to show the overall dispersion of the slip vector azimuths.

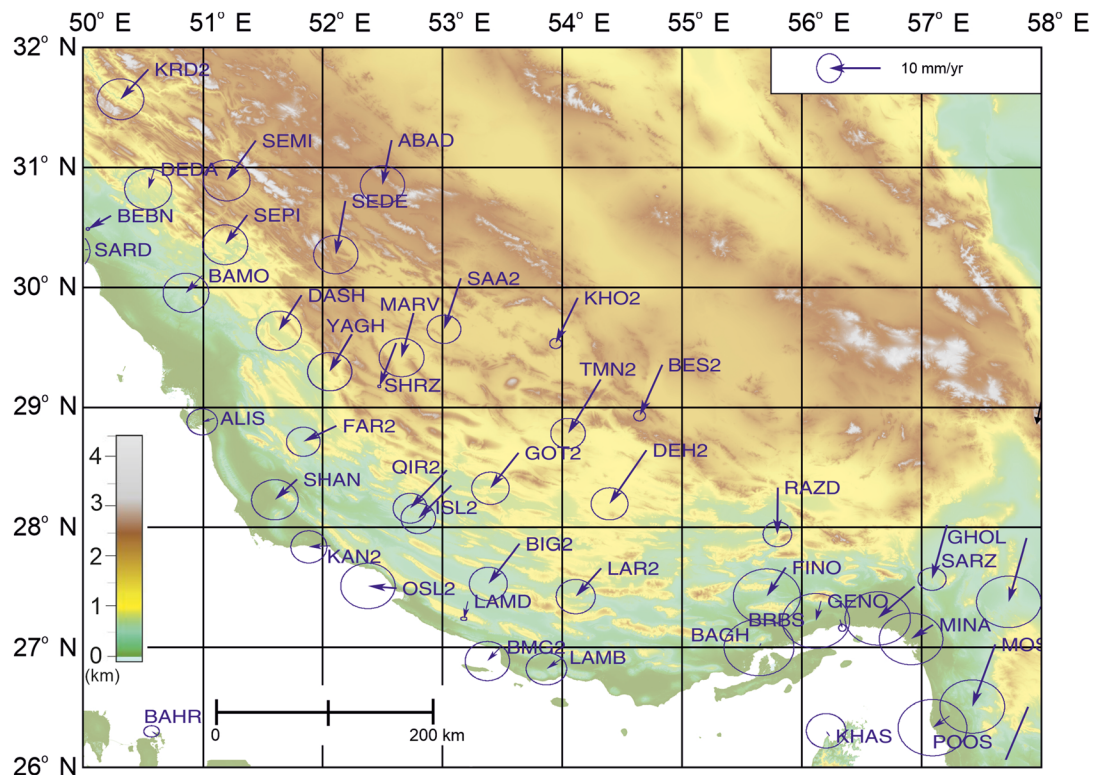


**Figure 7.** GPS-derived velocities relative to the Arabian Plate (and their 95% confidence ellipses), based on data in Khorrami et al. (2019).

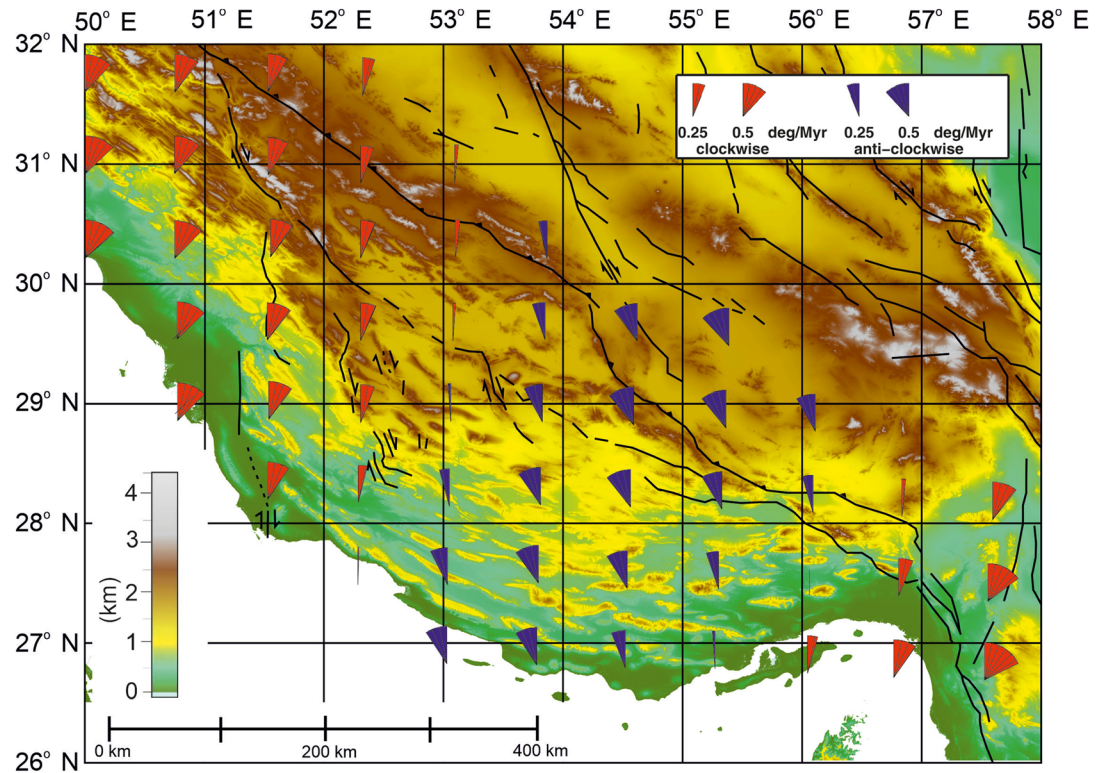


**Figure 8.** GPS vertical axis rotation rates for the study area. Rotation rates were calculated on a 75 km × 75 km rectangular grid. Results define two broad regions in the Zagros, of clockwise rotations west of 53°E, and counterclockwise to the east. Uncertainties for the rotation rates range between  $\pm 0.0005^\circ$  and  $\pm 0.08^\circ \text{ Myr}^{-1}$  for whole study area and for the central Zagros are  $\sim 0.02^\circ \text{ Myr}^{-1}$ .

more complicated. The westernmost limit of the fold trace trends WNW-ESE, and across the culmination of the anticline, which is affected by a salt diapir, there is a continuation of this trend, with a well-exposed fold closure preserved in limestones of the Guri Member of the Mishan Formation (Early to early Middle Miocene age) (Figure 4a). Qeshm Island (Figure 4b) also displays two fold trends in the same local area. Most of the length of the island consists of three anticlines, each trending ENE-WNW: Salakh, Suza, and Holor. Exposed strata are largely from the Miocene-Pliocene Mishan and Agha Jari formations. The Left Anticline trends NW-SE, and the southeastern nose of this structure is separated from the Suza Anticline by the Ramkan Syncline (Nissen et al., 2010). Where anticlines in Figure 4 intersect each other there are domal structures, with the additional factor of a Hormuz salt diapir within the Shab Anticline (Figure 4a). The domes are picked out both by present topography and the outcrop pattern of the deformed stratigraphy (Figure 4c). There is no evidence that one orientation of fold represents a different generation to another, for example, a youthful generation of active folds superimposed on mature, eroded, older folds.

We do not confirm the activity of a series of ENE-WSW left-lateral strike-slip faults suggested by Hessami et al. (2001) to deform eastern Fars. While there are linear alignments of salt diapirs that suggest some structural control with this orientation, there is little or no indication of active fault slip. Nor do reliable left-lateral focal mechanisms occur in this region (Nissen et al., 2011; Talebian & Jackson, 2004 and references therein). If active left-lateral slip occurs in this region, the surface expression is very different to the sharply defined, seismically active, right-lateral faults further west, such as the Kazerun Fault (Authemayou et al., 2006; Koyi et al., 2016).

Thrust earthquake slip vectors for the whole Fars Arc have an average azimuth of  $191^\circ \pm 21^\circ$ , using the slip vector measured toward the Arabian Plate (Table 1; Figure 6). There is a regional variation in azimuths. West of 53°E, the average azimuth is  $213^\circ \pm 23^\circ$ ; east of 53°E, the average is  $187^\circ \pm 18^\circ$ . Azimuths are variable within small areas in eastern Fars, with differences of up to 90° for events located within 50 km of each other (Figure 6). There is a distinct cluster of thrust earthquakes in the easternmost part of Fars, with slip azimuths

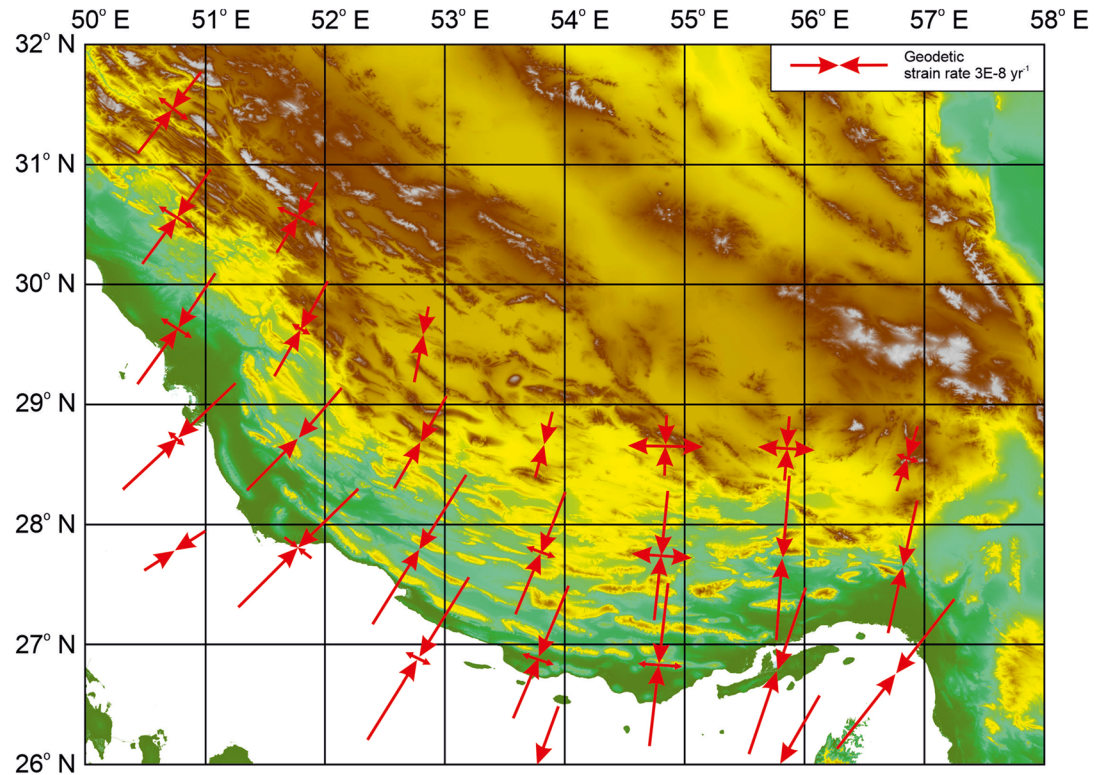


**Figure 9.** Geodetic strain axes for the Fars Arc, eastern Zagros, from Raeesi et al. (2017), for comparison with other kinematic data presented in Figures 6 and 7 and summarized in Figure 10. The average uncertainties for strain rates are  $\pm 3 \times 10^{-9} \text{ yr}^{-1}$  for the shortening rate and  $\pm 4 \times 10^{-10} \text{ yr}^{-1}$  for the extension rate.

toward the southeast (i.e., northeast-southwest striking fault planes). These events are close to, but distinct from, the north-south striking fault system that marks the eastern limit of the Zagros and the Arabian Plate.

GPS velocity data (Figure 7) show vectors in an Arabian reference frame with a maximum of  $\sim 10 \text{ mm yr}^{-1}$  of NNE-SSW shortening across the Zagros, south of the Arabia-Eurasia suture (Hessami et al., 2006; Vernant et al., 2004). The average azimuth is  $215^\circ \pm 23^\circ$  in an Arabian Plate reference frame. There is a minor divergence in azimuths between western and eastern Fars (Khorrami et al., 2019; Nilforoushan & Koyi, 2007), but this is less than for the earthquake slip vectors: The average azimuth west of  $53^\circ\text{E}$  is  $221^\circ \pm 28^\circ$ , and  $208^\circ \pm 13^\circ$  for data points to the east of  $53^\circ\text{E}$ . Strain rates derived from the GPS data set (Raeesi et al., 2017) (Figure 9) are very similar to the other strain data summarized in Table 1. The direction of the maximum strain axes changes from almost orthogonal to the strike of the Zagros in the south to a NW-SE direction in the western part of the Fars Arc. The azimuths of the maximum strain axes are generally perpendicular to the fold axes in the Fars region.

**Table 1**  
*Kinematic Data for the Fars Arc*

	Overall Fars Arc		West of $53^\circ\text{E}$		East of $53^\circ\text{E}$	
	Average	Standard deviation	Average	Standard deviation	Average	Standard deviation
Orthogonal directions to fold trends	204°	15°	218°	25°	189°	20°
Thrust earthquake slip vector azimuths	191°	21°	213°	23°	187°	18°
GPS vector azimuths	215°	23°	221°	28°	208°	13°
Maximum geodetic strain axis orientation	202°	52°	216°	53°	192°	53°

*Note.* Geodetic strain axis orientations are from Raeesi et al. (2017).

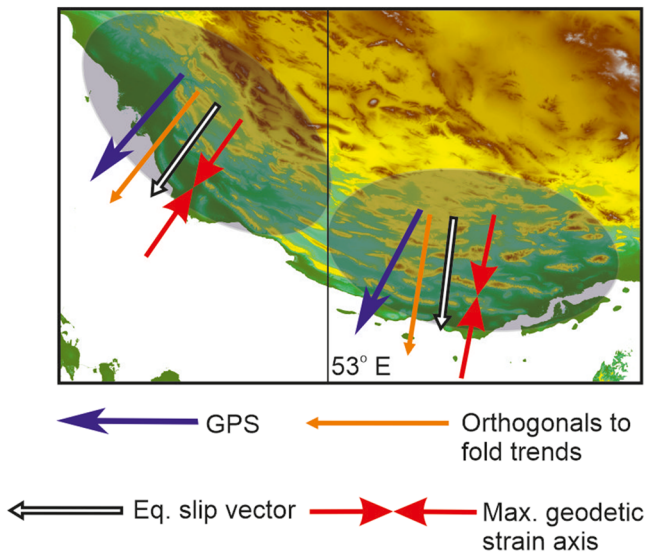


**Figure 10.** Summary of kinematic data for the Fars Arc west and east of 53°E, from data in Table 1; arrows represent summaries of regional data, from the areas roughly defined by the gray ovals. Whereas the thrust earthquake slip vectors, orthogonal directions to fold trends, and strain axes are all independent of any reference frame, GPS velocities are in an Arabian Plate reference frame. Orientations of all data sets are aligned in western Fars (west of 53° E), but not in the east; there is no significant spread in the GPS data, but there is an overall counterclockwise rotation visible in the other data sets.

these models. For example, the present-day kinematics within the fold-and-thrust belt can be compared with the regional obliquity of convergence, or structural evidence for intersection of different segments. It is an outstanding question over what time scales the present picture is representative and how short-term and long-term patterns of deformation compare with each other. In this paper, we argue for gravitational spreading being the most likely cause of curvature in the Fars Arc, but our focus is on the kinematics and how this curvature is achieved, rather than the underlying dynamic cause.

### 5.1. Rotation Within the Fars Arc

Although Copley (2012) was correct in summarizing the Zagros as a linear belt overall, this is a simplification: The Fars Arc justifies its name, given the arcuate pattern of fold orientations across the region from west to east (Figure 3). A key observation is that there is an overall fanning-out of the orthogonal directions to the fold trends, thrust earthquake slip vector azimuths and instantaneous strain axes (Figures 5 and 9), that is greater than the spread in the GPS velocity data (Table 1; Figure 7), summarized in Figure 10. In western Fars, there is alignment between the equivalent data sets. While this alignment might look like a simple kinematic system, the active right-lateral faulting and clockwise vertical axis rotation also need to be considered. We suggest that the regional clockwise rotation is mainly taken up by the right-lateral faults in the region, such as the Kazerun Fault. Counterclockwise rotations of individual folds against these faults act to counterbalance the regional rotation (Authemayou et al., 2006), leaving the finite strain markers (folds) and instantaneous strain markers in alignment (Figure 11).

GPS-derived convergence toward ~208° in eastern Fars can be achieved by a combination of thrusts with average slip vectors toward ~187°, coupled with counterclockwise rotations of the predominant ENE-WSW fault blocks (Figure 11), similar to other examples within continental interiors (e.g., Bayasgalan et al., 2005): Slip along the fault planes (recorded by the focal mechanisms) acts in concert with the vertical axis rotations (which are not recorded by focal mechanisms), to produce the overall convergence direction seen in the GPS data. Overall curvature of the Fars Arc increases by the cumulative effect of small-scale, vertical axis, block rotations. These rotations are dominantly, but not universally, clockwise in the west and counterclockwise in the east (Figure 3), so that the simple overall rotation sense given by the

The geodetic rotation rate map (Figure 8) shows two distinctive regions in the Fars Arc, with opposite rotation sense; the changeover in rotation sense occurs at the 53°E meridian. Interestingly, this line is to the west of the apex of the Arc, at ~54°E. From the Markan-Zagros transition zone in the southeast to the central Zagros (between longitudes ~53° to ~56°E), rotations are counterclockwise, whereas west of 53°E, there are clockwise rotations. The changeover of rotation sense occurs at the eastern limit of the array of right-lateral strike-slip faults in western Fars. Rotation rates are variable, with a maximum rate of ~0.5° Myr<sup>-1</sup>. Rotation sense is clockwise to the east of the Fars Arc, beyond 56.5°E (Figure 8), as noted by Bayer et al. (2006).

## 5. Discussion

Fold-and-thrust belts are commonly curved in plan view, and the nature and origins of this curvature have been the subject of many studies (e.g., Copley, 2012; Hindle & Burkhard, 1999; Macedo & Marshak, 1999; Marques & Cobbold, 2006; Styron et al., 2011). We consider three main hypotheses for the mechanisms that cause orogenic curvature. High topography may cause gravitational spreading over the foreland and an arcuate shape (Copley, 2012), enhanced by a weak décollement layer (Nilforoushan & Koyi, 2007). Alternatively, curvature may occur where two segments of an orogen intersect at an angle and overlap (Macedo & Marshak, 1999) or to accommodate oblique plate convergence (Styron et al., 2011). Our study has focused on neotectonic data, in the form of the recent earthquake record and geodetic (GPS) data, because of the power these provide in analyzing the regional kinematics, and testing

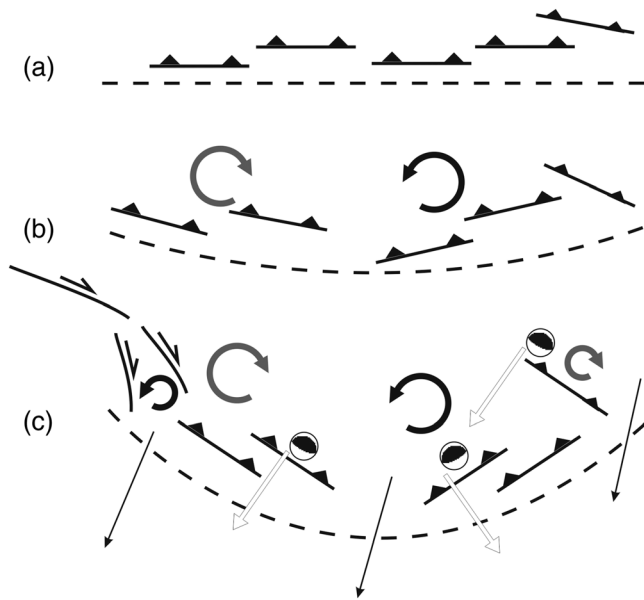


**Figure 11.** Schematic illustration of long-term, progressive curvature development of a fold-and-thrust belt through vertical axis rotations of thrusts and the fault blocks they define (a–c), to explain the kinematics and deformation of the Fars Arc. Overall clockwise rotation in the west and counterclockwise rotation in the east mask local rotations that can take place in the opposite sense in each area. Circular arrows, vertical axis rotations; open arrows, earthquake slip vector azimuths; thin black arrows, GPS velocities; dashed line, Zagros deformation front. (a) Initial, linear state. (b) Intermediate stage, with opposing sense of rotation within each side of the fold-and-thrust. (c) Mature stage, equivalent to the present Fars Arc.

faults in this region, if strike-slip motion is simply a consequence of the rotation. If left-lateral faults exist as depicted by Koyi et al. (2016), they are either inactive or, like western Fars, the process of producing the overall fold-and-thrust belt curvature is more important than passive “bookshelf” rotations of rigid blocks (Figure 12). We conclude that the generation of fold-and-thrust belt curvature dominates over along-strike lengthening, to produce the observed right-lateral faulting and clockwise rotations in western Fars (Authemayou et al., 2006; Lacombe et al., 2006).

There is a difference between the western and eastern parts of the Fars Arc in that right-lateral faults are clearly expressed in the west, but, as noted above, left-lateral counterparts in the east do not seem to be present or, at least, not active. This may relate to the overall obliquity of convergence at the plate scale and the need for a greater component of strain partitioning in western Fars and indeed parts of the Zagros west of the Fars Arc altogether (Authemayou et al., 2006; Talebian & Jackson, 2002).

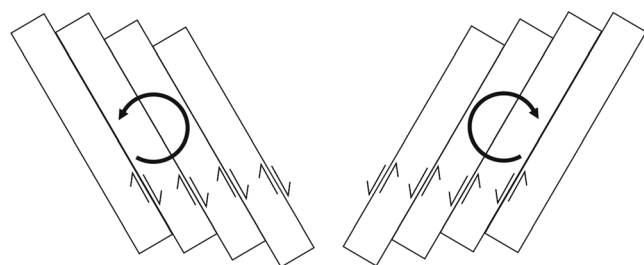


**Figure 12.** Previous predictions of counterclockwise vertical axis rotations in western Fars (Talebian & Jackson, 2004) and clockwise rotations in eastern Fars (Koyi et al., 2016), as the result of passive “bookshelf” models. Geodetic data reveal the opposite overall sense of rotation is occurring in each area (Figure 8).

GPS data is superimposed on the more complex picture provided by paleomagnetic results (Aubourg et al., 2010).

These small-scale rotations are not present in the original end-member schemes of Hindle and Burkhard (1999) for arcuate fold-and-thrust belts (Figure 1). The Fars Arc shows aspects of both “Piedmont glacier” and “Primary arc” styles, in that if only the GPS data were considered it might be considered to be of the “Primary arc” type (Figure 7), while the more divergent earthquake slip vectors give a resemblance to “Piedmont glacier” models (Figure 6).

The deformation of the Fars Arc resembles the rotating faults and fault blocks of the active Aegean arc (Taymaz et al., 1991), with the obvious difference that the Zagros is in overall compression, while the Aegean region is rapidly extending. It is notable that the present-day, overall rotation rates recorded in the GPS velocity field (Figure 8) on a  $75 \times 75$  km grid are distinctly smaller ( $\leq 0.5^\circ \text{ Myr}^{-1}$ ) than the long-term rotation rates recorded in paleomagnetic data (up to  $2^\circ \text{ Myr}^{-1}$ ; Aubourg et al., 2008). Presumably, the latter represent more rapid, localized variations, including blocks that rotate in an opposite sense to the regional sense in the west and east halves of the Fars Arc (Figure 11).

Hessami et al. (2001) and Talebian and Jackson (2004) predicted counterclockwise rotations in the western Fars region, to achieve along-strike lengthening of the Zagros during right-lateral slip on the Kazerun Fault and similar faults to its east (Figure 12). There would be left-lateral slip on ~NW-SE faults, if strike-slip was simply the passive result of two-dimensional fault block rotation in the clockwise sense recorded by the GPS data (Figure 12). Such left-lateral slip does not occur.

Counterclockwise rotation in the eastern part of the study area, east of  $53^\circ\text{E}$  (Figure 8), should produce right-lateral strike-slip on any NE-SW faults in this region, if strike-slip motion is simply a consequence of the rotation. If left-lateral faults exist as depicted by Koyi et al. (2016), they are either inactive or, like western Fars, the process of producing the overall fold-and-thrust belt curvature is more important than passive “bookshelf” rotations of rigid blocks (Figure 12). We conclude that the generation of fold-and-thrust belt curvature dominates over along-strike lengthening, to produce the observed right-lateral faulting and clockwise rotations in western Fars (Authemayou et al., 2006; Lacombe et al., 2006).

## 5.2. Distinction of the Fars Arc Within the Zagros

The question follows: Why does deformation in the Fars Arc differ from the rest of the Zagros (Figure 2), where there is not an arcuate shape to the fold-and-thrust belt? One clear control is the structural boundary at the eastern end of the Fars Arc, where Zagros collisional convergence transfers into the active subduction under the Makran region (Aubourg et al., 2008; Bayer et al., 2006; Regard et al., 2005). The western end of the Fars Arc does not seem to mark such a pronounced tectonic transition, but observations suggest basement structure plays a role in controlling the style of the active tectonics, including limiting the lateral extent of the Fars Arc. The first observation is that the Hormuz Series salt does not appear in

diapirs within the SFB, west of the Kazerun Fault (Figure 3; Talbot & Alavi, 1996). This salt distribution has previously been suggested as allowing the propagation of deformation further southward within the Fars Arc (Aubourg et al., 2008; Authemayou et al., 2006; Leturmy et al., 2010; Nilfouroushan & Koyi, 2007). It is unlikely that the distribution of salt is the only factor, however, given that the Zagros basement beneath the salt is also actively deforming, as evidenced by the seismicity record (Nissen et al., 2011; Talebian & Jackson, 2004). Based on thermal-mechanical modeling results (Nilfouroushan et al., 2013), the salt décollement in eastern Zagros can decouple the basement and cover sediments deformation to different extents, depending on its thickness. The diapir-free region within the Fars Arc shows no signs that it deforms differently to adjacent regions (Figure 3), which is a separate argument against the salt playing a major role in controlling regional structure.

Another factor is that west of the Kazerun Fault, late Cenozoic deformation seems to have been established near its present southwestern limit as long ago as ~8 Ma (Homke et al., 2004) and been unsuccessful in propagating further toward the foreland since this time. Active deformation is limited to the northeast of the line referred to in the Iraqi Zagros as the boundary between the Stable and Unstable Shelf sequences—a reference to the deeper-water nature of Mesozoic (i.e., precollisional) sedimentary units in the northeast of the Arabian Plate (Jassim & Goff, 2006). It is not clear that such a constraint operates to the east of the Kazerun Fault; there is no indication of a precollisional feature that restricts the southward-propagation of the fold-and-thrust belt. In summary, we suggest the Fars Arc deformation is sufficiently restricted at its eastern and western margins, compared with the intervening region, to impart the present curvature (Aubourg et al., 2008).

Previous studies (e.g., Leturmy et al., 2010; Molinaro et al., 2005) have proposed that structures within the eastern Fars region record two distinct phases of deformation, which are suggested to be an early phase of detached (thin-skinned) thrusting and folding, superceded by a basement-involved (thick-skinned) phase, which continues to the present day. The results of this study, in particular the earthquake slip vector dispersion (Figure 6) and the evidence for contemporary folding of different orientations (Figure 4), suggest that variable orientations of synchronous folding and thrusting achieve overall north-south convergence across the Fars Arc as described above (Figure 11). There is no requirement for separate deformation events with different stress orientations. It is unlikely that this process to create fold interference patterns is unique to the Fars Arc, and future studies of similar interference patterns in other regions should consider the possibility that they record deformation during a single phase of compression, rather than the superposition of different stress regimes, with different orientations at different times. This scenario is especially likely when there is no independent evidence of a regional change in plate convergence direction during deformation.

In this study, we have compared the results of neotectonic geodetic and seismicity observations of the Fars Arc to data that represent the longer-term evolution of the range, namely, fold orientations and paleomagnetic data. Where differences exist, it is potentially a consequence of the spatial scale of each type of observation rather than the time scale: The location of GPS stations, their distributions around faults, and the gridding distance can all affect results. This may explain why the regional GPS data are not consistent with paleomagnetic records in some parts of the Zagros (Figure 3). But time scales are no doubt also important. Our model (Figure 11) predicts that the Fars Arc becomes more curved over time, convex southward, but the rate at which this curvature is achieved is not well constrained. Future work could also address the implications of the late Cenozoic tectonic reorganization of the collision zone for the Fars Arc.

### 5.3. Comparisons With Other Arcuate Fold-and-Thrust Belts

The Zagros crust seems weak compared with many other continental regions. For example, fault lengths are shorter, and earthquakes are of lower magnitude than in the Himalaya (Hatzfeld & Molnar, 2010; Ramsey et al., 2008). This weakness may be the result of the relative youth of the Arabian Plate basement and the protracted rift history of the northern side of the plate, with these rifting events defining the structures that have been reactivated in the Cenozoic during the Arabia-Eurasia collision. It means that the Zagros deforms by a large number of rather small (~20–40 km) separate faults, with weak linkages, rather than the longer structures of the Himalaya. The result is that the apparently smooth variation in structure around the Fars Arc is the sum of the differential movement of numerous short fault blocks, each of which is defined by the length of the faults that bound it, and each of which remains relatively linear, rather than progressive curvature of a smaller number of longer fault blocks.

There are potential lessons from the Fars Arc for understanding the behavior of other fold-and-thrust belts worldwide, with the caveat that only active examples can be examined via earthquake and geodetic data. We highlight the strongly curved Kepingtage fold-and-thrust belt at the southern side of the Tianshan, northwest China, where GPS vectors are consistent in azimuth (Yang et al., 2008), but thrust slip vectors show a fanning-out pattern (Allen et al., 1999); this region seems to show similar behavior to the Fars Arc.

#### 5.4. Kinematics and Dynamics of the Fars Arc

As a final subject, we consider the implications of our kinematic analysis for understanding the dynamics of the Fars Arc and the cause, rather than the mechanism, for fold-and-thrust belt curvature. Our work argues against the application of generic models that relate some fold-and-thrust belt curvature to the geometry of the foreland (Macedo & Marshak, 1999), because the curvature and block rotations are present throughout the Fars Arc and not only in the outer parts. The Styron et al. (2011) model for the Himalaya related curvature to strain partitioning in that range, but the Zagros does not display curvature where plate convergence is more oblique, in the northwest, such that this model is unlikely to apply to the Fars Arc.

Two factors favor the gravitational spreading model (Copley, 2012) operating in the Fars Arc to explain the overall curvature. First, the interior of the Iranian Plateau has surface elevations on the order of  $\sim 2$  km above sea level, such that there is a component of gravitational potential energy in the system. Second, the crust of the Zagros is relatively weak, given the seismicity record of relatively small earthquakes rather than events on the scale of the Himalaya (i.e.,  $M < 7$ ). Weaker crust would favor the spreading mechanism. Additionally, the Fars region is laterally restricted by the tectonic boundaries at its western and eastern margins (e.g., Aubourg et al., 2010). In combination, these factors suggest that there has been a process of gravitational spreading of the Fars Arc toward the foreland (in the style proposed by Copley (2012)), but this process is laterally restricted by preexisting tectonic boundaries. Therefore, the Fars Arc contains elements of both the “Piedmont glacier” and “Primary arc” models (Hindle & Burkhard, 1999) while containing rotating fault blocks that feature in neither of these models.

## 6. Conclusions

An analysis of kinematic data for the Fars Arc reveals a greater spread in the orthogonal directions to fold trends, thrust slip vector azimuths (Figure 6) and instantaneous strain axes (Figure 9) than the GPS velocities (Table 1; Figure 7), summarized in Figure 10. Rotation rates derived from the GPS data (Figure 8) are  $\leq 0.5^\circ \text{ Myr}^{-1}$ , which is lower than likely long-term rates, derived from paleomagnetic studies (Aubourg et al., 2008) of  $\sim 1\text{--}2^\circ \text{ Myr}^{-1}$  (Figure 3). We attribute these structural patterns to deformation being restricted at the eastern end of the collision zone, at the Zagros/Makran transition, and at the Kazerun Fault, which marks a precollisional basement structure within the Zagros (Aubourg et al., 2010; Talbot & Alavi, 1996). Fault blocks within the Fars Arc rotate about vertical axes to achieve the overall curvature, predominantly clockwise in the west and counterclockwise in the east, but with considerable local variation (Figure 3). The active, GPS-derived rotations are of the opposite sense to previous predictions based on the presence of right-lateral faults in western Fars (Hessami et al., 2001; Talebian & Jackson, 2004) and the interpretation of left-lateral faults in eastern Fars (Koyi et al., 2016) but consistent with the Fars Arc becoming more arcuate over time (Figure 11).

Western and eastern Fars are not perfect mirror images of each other. Prominent, seismically active, right-lateral faults in western Fars have no counterparts in the east (Figure 3), whereas eastern Fars shows a variation between GPS velocities and strain orientations that does not occur in the west (Figure 10). The counterclockwise geodetic rotation sense in eastern Fars is consistent with the mismatch between GPS and thrust slip vector azimuths, if the rotation is achieved by ENE-WSW trending fault blocks. The present alignment of structural and kinematic data in western Fars is consistent with the clockwise rotation being largely achieved on the right-lateral faults in this region, with local counterclockwise rotations of folds where they abut or are cross-cut by these faults.

Different fault and fold orientations are active at the same time within localized areas, especially in eastern Fars, with examples of mutually cross-cutting folds (Figure 4). Domal fold interference patterns are not caused by superposed deformation events with different stress orientations, and there is no requirement that the Zagros underwent a tectonic transition from thin-skinned to thick-skinned deformation over time.

## Data Availability Statement

Data sets for this research are included in these papers (and their supplementary information files): Khorrami et al. (2019); Talebian and Jackson (2004); Nissen et al. (2011), with data from the Global CMT catalog (Dziewonski et al., 1981; Ekström et al., 2012).

## Acknowledgments

We thank Hemin Koyi for helpful comments on an early draft of the manuscript. M. B. A. is grateful to the Geological Survey of Iran for discussions on the regional tectonics. We used SSPX and GMT for computing and plotting geodetic rotation rates. We thank John Weber, an anonymous reviewer, and the associate editor for their helpful reviews. The content in this academic paper represents the opinions of the authors and is a product of professional research. It does not represent the position or opinions of the Office for Nuclear Regulation nor the official position of any staff members.

## References

- Agard, P., Omrani, J., Jolivet, L., Whitechurch, H., Vrielynck, B., Spakman, W., et al. (2011). Zagros orogeny: A subduction-dominated process. *Geological Magazine*, *148*, 692–725. <https://doi.org/10.1017/s001675681100046x>
- Allen, M. B., & Armstrong, H. A. (2008). Arabia-Eurasia collision and the forcing of mid Cenozoic global cooling. *Palaeogeography Palaeoclimatology Palaeoecology*, *265*, 52–58. <https://doi.org/10.1016/j.palaeo.2008.04.021>
- Allen, M. B., Saville, C., Blanc, E. J.-P., Talebian, M., & Nissen, E. (2013). Orogenic plateau growth: Expansion of the Turkish-Iranian Plateau across the Zagros fold-and-thrust belt. *Tectonics*, *32*, 171–190. <https://doi.org/10.1002/tect.20025>
- Allen, M. B., Vincent, S. J., & Wheeler, P. J. (1999). Late Cenozoic tectonics of the Kepingtage thrust zone: Interactions of the Tien Shan and Tarim Basin, northwest China. *Tectonics*, *18*, 639–654. <https://doi.org/10.1029/1999tc900019>
- Allmendinger, R. W., Reillinger, R., & Loveless, J. (2007). Strain and rotation rate from GPS in Tibet, Anatolia, and the Altiplano. *Tectonics*, *26*, TC3013. <https://doi.org/10.1029/2006tc002030>
- Altamimi, Z., Métivier, L., & Collilieux, X. (2012). ITRF2008 plate motion model. *Journal of Geophysical Research*, *117*. <https://doi.org/10.1029/2011JB008930>
- Aubourg, C., Smith, B., Bakhtari, H. R., Guya, N., & Eshraghi, A. (2008). Tertiary block rotations in the Fars Arc (Zagros, Iran). *Geophysical Journal International*, *173*, 659–673. <https://doi.org/10.1111/j.1365-246x.2008.03732.x>
- Aubourg, C., Smith, B., Eshraghi, A., Lacombe, O., Authemayou, C., Amrouch, K., et al. (2010). New magnetic fabric data and their comparison with palaeostress markers in the Western Fars Arc (Zagros, Iran): Tectonic implications. In P. Leturmy, & C. Robin (Eds.), *Tectonic and stratigraphic evolution of Zagros and Makran during the Mesozoic-Cenozoic* (pp. 97–120). Bath: Geological Soc Publishing House.
- Austermann, J., & Iaffaldano, G. (2013). The role of the Zagros orogeny in slowing down Arabia-Eurasia convergence since similar to 5 Ma. *Tectonics*, *32*, 351–363. <https://doi.org/10.1002/tect.20027>
- Authemayou, C., Chardon, D., Bellier, O., Malekzadeh, Z., Shabaniyan, E., & Abbassi, M. R. (2006). Late Cenozoic partitioning of oblique plate convergence in the Zagros fold-and-thrust belt (Iran). *Tectonics*, *25*, Tc3002. <https://doi.org/10.1029/2005tc001860>
- Bahroudi, A., & Koyi, H. (2003). Effect of spatial distribution of Hormuz salt on deformation style in the Zagros fold and thrust belt: An analogue modelling approach. *Journal of the Geological Society, London*, *160*, 719–733. <https://doi.org/10.1144/0016-764902-135>
- Bakhtari, H. R., de Lamotte, D. F., Aubourg, C., & Hassanzadeh, J. (1998). Magnetic fabrics of Tertiary sandstones from the Arc of Fars (Eastern Zagros, Iran). *Tectonophysics*, *284*, 299–316. [https://doi.org/10.1016/s0040-1951\(97\)00179-0](https://doi.org/10.1016/s0040-1951(97)00179-0)
- Barber, D. E., Stockli, D. F., Horton, B. K., & Koshnaw, R. I. (2018). Cenozoic exhumation and foreland basin evolution of the Zagros orogen during the Arabia-Eurasia collision, western Iran. *Tectonics*, *37*, 4396–4420. <https://doi.org/10.1029/2018tc005328>
- Bayasgalan, A., Jackson, J., & McKenzie, D. (2005). Lithosphere rheology and active tectonics in Mongolia: Relations between earthquake source parameters, gravity and GPS measurements. *Geophysical Journal International*, *163*, 1151–1179. <https://doi.org/10.1111/j.1365-246x.2005.02764.x>
- Bayer, R., Chery, J., Tatar, M., Vernant, P., Abbassi, M., Masson, F., et al. (2006). Active deformation in Zagros-Makran transition zone inferred from GPS measurements. *Geophysical Journal International*, *165*, 373–381. <https://doi.org/10.1111/j.1365-246x.2006.02879.x>
- Berberian, M. (1995). Master "blind" thrust faults hidden under the Zagros folds: Active basement tectonics and surface morphotectonics. *Tectonophysics*, *241*, 193–224. [https://doi.org/10.1016/0040-1951\(94\)00185-c](https://doi.org/10.1016/0040-1951(94)00185-c)
- Blanc, E. J.-P., Allen, M. B., Inger, S., & Hassani, H. (2003). Structural styles in the Zagros Simple Folded Zone, Iran. *Journal of the Geological Society, London*, *160*, 400–412. <https://doi.org/10.1144/0016-764902-110>
- Cardozo, N., & Allmendinger, R. W. (2009). SSPX: A program to compute strain from displacement/velocity data. *Computers & Geosciences*, *35*, 1343–1357. <https://doi.org/10.1016/j.cageo.2008.05.008>
- Copley, A. (2012). The formation of mountain range curvature by gravitational spreading. *Earth and Planetary Science Letters*, *351*, 208–214. <https://doi.org/10.1016/j.epsl.2012.07.036>
- Dziewonski, A. M., Chou, T.-A., & Woodhouse, J. H. (1981). Determination of earthquake source parameters from waveform data for studies of global and regional seismicity. *Journal of Geophysical Research*, *86*(B4), 2825–2852. <https://doi.org/10.1029/jb086ib04p02825>
- Ekström, G., Nettles, M., & Dziewonski, A. M. (2012). The global CMT project 2004–2010: Centroid-moment tensors for 13,017 earthquakes. *Physics of the Earth and Planetary Interiors*, *200-201*, 1–9. <https://doi.org/10.1016/j.pepi.2012.04.002>
- Engdahl, E. R., Jackson, J. A., Myers, S. C., Bergman, E. A., & Priestley, K. (2006). Relocation and assessment of seismicity in the Iran region. *Geophysical Journal International*, *167*, 761–778. <https://doi.org/10.1111/j.1365-246x.2006.03127.x>
- Fakhari, M. D., Axen, G. J., Horton, B. K., Hassanzadeh, J., & Amini, A. (2008). Revised age of proximal deposits in the Zagros foreland basin and implications for Cenozoic evolution of the High Zagros. *Tectonophysics*, *451*, 170–185. <https://doi.org/10.1016/j.tecto.2007.11.064>
- Falcon, N. (1974). In A. Spencer (Ed.), *Southern Iran: Zagros mountains, in Mesozoic-Cenozoic orogenic belts: Data for orogenic studies* (pp. 199–211). London: Special Publication of the Geological Society of London.
- Hatzfeld, D., Authemayou, C., van der Beek, P., Bellier, O., Lave, J., Oveisi, B., et al. (2010). The kinematics of the Zagros Mountains (Iran). In P. Leturmy, & C. Robin (Eds.), *Tectonic and stratigraphic evolution of Zagros and Makran during the Mesozoic-Cenozoic* (pp. 19–42). Bath: Geological Soc Publishing House.
- Hatzfeld, D., & Molnar, P. (2010). Comparisons of the kinematics and deep structures of the Zagros and Himalaya and of the Iranian and Tibetan plateaus and geodynamic implications. *Reviews of Geophysics*, *48*, Rg2005. <https://doi.org/10.1029/2009rg000304>
- Hessami, K., Koyi, H. A., & Talbot, C. J. (2001). The significance of strike-slip faulting in the basement of the Zagros fold and thrust belt. *Journal of Petroleum Geology*, *24*, 5–28. <https://doi.org/10.1111/j.1747-5457.2001.tb00659.x>
- Hessami, K., Nilforoushan, F., & Talbot, C. J. (2006). Active deformation within the Zagros Mountains deduced from GPS measurements. *Journal of the Geological Society*, *163*, 143–148. <https://doi.org/10.1144/0016-764905-031>
- Hindle, D., & Burkhard, M. (1999). Strain, displacement and rotation associated with the formation of curvature in fold belts; the example of the Jura arc. *Journal of Structural Geology*, *21*(8–9), 1089–1101. [https://doi.org/10.1016/s0191-8141\(99\)00021-8](https://doi.org/10.1016/s0191-8141(99)00021-8)

- Homke, S., Vergés, J., Garcés, M., Emami, H., & Karpuz, R. (2004). Magnetostratigraphy of Miocene–Pliocene Zagros foreland deposits in the front of the Push-e Kush Arc (Lurestan Province, Iran). *Earth and Planetary Science Letters*, *225*, 397–410. <https://doi.org/10.1016/j.epsl.2004.07.002>
- Jackson, J. (2001). Living with earthquakes: Know your faults. *Journal of Earthquake Engineering*, *5*, 5–123. <https://doi.org/10.1080/13632460109350530>
- Jackson, J., Priestley, K., Allen, M., & Berberian, M. (2002). Active tectonics of the South Caspian Basin. *Geophysical Journal International*, *148*, 214–245. <https://doi.org/10.1046/j.1365-246x.2002.01005.x>
- Jahani, S., Callot, J. P., de Lamotte, D. F., Letouzey, J., & Leturmy, P. (2007). The salt diapirs of the eastern Fars province (Zagros, Iran): A brief outline of their past and present. In O. Lacombe, J. Lave, F. Roure, & J. Vergés (Eds.), *Thrust belts and foreland basins: From fold kinematics to hydrocarbon systems* (pp. 289–308). Berlin: Springer-Verlag Berlin.
- Jassim, S. Z., & Goff, J. C. (2006). Phanerozoic development of the northern Arabian Plate. In S. Z. Jassim, & J. C. Goff (Eds.), *Geology of Iraq* (pp. 32–44). Prague: Dolin.
- Kent, P. E. (1979). The emergent Hormuz salt plugs of southern Iran. *Journal of Petroleum Geology*, *2*, 117–144. <https://doi.org/10.1111/j.1747-5457.1979.tb00698.x>
- Khorrani, F., Vernant, P., Masson, F., Nilfouroushan, F., Mousavi, Z., Nankali, H., et al. (2019). An up-to-date crustal deformation map of Iran using integrated campaign-mode and permanent GPS velocities. *Geophysical Journal International*, *217*, 832–843. <https://doi.org/10.1093/gji/ggz045>
- Koshnaw, R. I., Stockli, D. F., & Schlunegger, F. (2019). Timing of the Arabia-Eurasia continental collision—Evidence from detrital zircon U–Pb geochronology of the Red Bed Series strata of the northwest Zagros hinterland, Kurdistan region of Iraq. *Geology*, *47*, 47–50. <https://doi.org/10.1130/g45499.1>
- Koyi, H., Nilfouroushan, F., & Hessami, K. (2016). Modelling role of basement block rotation and strike-slip faulting on structural pattern in cover units of fold-and-thrust belts. *Geological Magazine*, *153*, 827–844. <https://doi.org/10.1017/s0016756816000595>
- Lacombe, O., Bellahsen, N., & Mouthereau, F. (2011). Fracture patterns in the Zagros Simply Folded Belt (Fars, Iran): Constraints on early collisional tectonic history and role of basement faults. *Geological Magazine*, *148*, 940–963. <https://doi.org/10.1017/s001675681100029x>
- Lacombe, O., Mouthereau, F., Kargar, S., & Meyer, B. (2006). Late Cenozoic and modern stress fields in the western Fars (Iran): Implications for the tectonic and kinematic evolution of central Zagros. *Tectonics*, *25*, TC1003. <https://doi.org/10.1029/2005TC001831>
- Leturmy, P., Molinaro, M., & de Lamotte, D. F. (2010). Structure, timing and morphological signature of hidden reverse basement faults in the Fars Arc of the Zagros (Iran). In P. Leturmy, & C. Robin (Eds.), *Tectonic and stratigraphic evolution of Zagros and Makran during the Mesozoic-Cenozoic* (pp. 121–138). Bath: Geological Society Publishing House.
- Macedo, J., & Marshak, S. (1999). Controls on the geometry of fold-thrust belt salients. *Geological Society of America Bulletin*, *111*(12), 1808–1822. [https://doi.org/10.1130/0016-7606\(1999\)111<1808:cotgof>2.3.co;2](https://doi.org/10.1130/0016-7606(1999)111<1808:cotgof>2.3.co;2)
- Marques, F. O., & Cobbold, P. R. (2006). Effects of topography on the curvature of fold-and-thrust belts during shortening of a 2-layer model of continental lithosphere. *Tectonophysics*, *415*(1–4), 65–80. <https://doi.org/10.1016/j.tecto.2005.12.001>
- McQuarrie, N. (2004). Crustal scale geometry of the Zagros fold-thrust belt, Iran. *Journal of Structural Geology*, *26*, 519–535. <https://doi.org/10.1016/j.jsg.2003.08.009>
- McQuarrie, N., Stock, J. M., Verdel, C., & Wernicke, B. (2003). Cenozoic evolution of Neotethys and implications for the causes of plate motions. *Geophysical Research Letters*, *30*, art. no. 2036(20). <https://doi.org/10.1029/2003GL017992>
- McQuarrie, N., & van Hinsbergen, D. J. J. (2013). Retrodeforming the Arabia-Eurasia collision zone: Age of collision versus magnitude of continental subduction. *Geology*, *41*, 315–318. <https://doi.org/10.1130/g33591.1>
- Molinaro, M., Leturmy, P., Guezou, J. C., de Lamotte, D. F., & Eshraghi, S. A. (2005). The structure and kinematics of the southeastern Zagros fold-thrust belt, Iran: From thin-skinned to thick-skinned tectonics. *Tectonics*, *24*, TC3007. <https://doi.org/10.1029/2004TC001633>
- Mouthereau, F. (2011). Timing of uplift in the Zagros belt/Iranian plateau and accommodation of late Cenozoic Arabia-Eurasia convergence. *Geological Magazine*, *148*, 726–738. <https://doi.org/10.1017/s0016756811000306>
- Mouthereau, F., Lacombe, O., & Vergés, J. (2012). Building the Zagros collisional orogen: Timing, strain distribution and the dynamics of Arabia/Eurasia plate convergence. *Tectonophysics*, *532*, 27–60. <https://doi.org/10.1016/j.tecto.2012.01.022>
- Mouthereau, F., Tensi, J., Bellahsen, N., Lacombe, O., De Boissroglier, T., & Kargar, S. (2007). Tertiary sequence of deformation in a thin-skinned/thick-skinned collision belt: The Zagros folded belt (Fars, Iran). *Tectonics*, *26*, TC5006. <https://doi.org/10.1029/2007TC002098>
- Nilfouroushan, F., & Koyi, H. A. (2007). Displacement fields and finite strains in a sandbox model simulating a fold-thrust-belt. *Geophysical Journal International*, *169*, 1341–1355. <https://doi.org/10.1111/j.1365-246x.2007.03341.x>
- Nilfouroushan, F., Pysklywec, R., Cruden, A., & Koyi, H. (2013). Thermal-mechanical modeling of salt-based mountain belts with pre-existing basement faults: Application to the Zagros fold and thrust belt, southwest Iran. *Tectonics*, *32*, 1212–1226. <https://doi.org/10.1002/tect.20075>
- Nissen, E., Tatar, M., Jackson, J. A., & Allen, M. B. (2011). New views on earthquake faulting in the Zagros fold-and-thrust belt of Iran. *Geophysical Journal International*, *186*, 928–944. <https://doi.org/10.1111/j.1365-246x.2011.05119.x>
- Nissen, E., Yamini-Fard, F., Tatar, M., Gholamzadeh, A., Bergman, E., Elliott, J. R., et al. (2010). The vertical separation of mainshock rupture and microseismicity at Qeshm island in the Zagros fold-and-thrust belt, Iran. *Earth and Planetary Science Letters*, *296*, 181–194. <https://doi.org/10.1016/j.epsl.2010.04.049>
- Obaid, A., & Allen, M. B. (2019). Landscape expressions of tectonics in the Zagros fold-and-thrust belt. *Tectonophysics*, *766*. <https://doi.org/10.1016/j.tecto.2019.05.024>
- Oveisi, B., Lave, J., van der Beek, P., Carcaillet, J., Benedetti, L., & Aubourg, C. (2009). Thick- and thin-skinned deformation rates in the central Zagros simple folded zone (Iran) indicated by displacement of geomorphic surfaces. *Geophysical Journal International*, *176*, 627–654. <https://doi.org/10.1111/j.1365-246x.2008.04002.x>
- Raeesi, M., Zarifi, Z., Nilfouroushan, F., Boroujeni, S. A., & Tiampo, K. (2017). Quantitative analysis of seismicity in Iran. *Pure and Applied Geophysics*, *174*, 793–833. <https://doi.org/10.1007/s00024-016-1435-4>
- Ramsey, L. A., Walker, R. T., & Jackson, J. (2008). Fold evolution and drainage development in the Zagros mountains of Fars province, SE Iran. *Basin Research*, *20*, 23–48. <https://doi.org/10.1111/j.1365-2117.2007.00342.x>
- Regard, V., Bellier, O., Thomas, J.-C., Bourlès, D., Bonnet, S., Abbassi, M. R., et al. (2005). Cumulative right-lateral fault slip rate across the Zagros-Makran transfer zone: Role of the Minab-Zendan fault system in accommodating Arabia-Eurasia convergence in southeast Iran. *Geophysical Journal International*, *162*, 177–203. <https://doi.org/10.1111/j.1365-246x.2005.02558.x>
- Ruh, J. B., Hirt, A. M., Burg, J. P., & Mohammadi, A. (2014). Forward propagation of the Zagros Simply Folded Belt constrained from magnetostratigraphy of growth strata. *Tectonics*, *33*, 1534–1551. <https://doi.org/10.1002/2013tc003465>

- Sarkarinejad, K., Zafarmand, B., & Oveisi, B. (2018). Evolution of the stress fields in the Zagros Foreland Folded Belt using focal mechanisms and kinematic analyses: The case of the Fars salient, Iran. *International Journal of Earth Sciences*, *107*, 611–633. <https://doi.org/10.1007/s00531-017-1516-3>
- Sella, G. F., Dixon, T. H., & Mao, A. (2002). REVEL: A model for recent plate velocities from space geodesy. *Journal of Geophysical Research*, *107*, art. no. 2081. <https://doi.org/10.1029/2000JB000033>
- Sherkati, S., Letouzey, J., & de Lamotte, D. F. (2006). Central Zagros fold-thrust belt (Iran): New insights from seismic data, field observation, and sandbox modeling. *Tectonics*, *25*, TC4007. <https://doi.org/10.1029/2004TC001766>
- Smith, B., Aubourg, C., Guezou, J. C., Nazari, H., Molinaro, M., Braud, X., & Guya, N. (2005). Kinematics of a sigmoidal fold and vertical axis rotation in the east of the Zagros-Makran syntaxis (southern Iran): Paleomagnetic, magnetic fabric and microtectonic approaches. *Tectonophysics*, *411*, 89–109. <https://doi.org/10.1016/j.tecto.2005.08.024>
- Styron, R. H., Taylor, M. H., & Murphy, M. A. (2011). Oblique convergence, arc-parallel extension, and the role of strike-slip faulting in the High Himalaya. *Geosphere*, *7*, 582–596. <https://doi.org/10.1130/ges00606.1>
- Talbot, C. J., & Alavi, M. (1996). The past of a future syntaxis across the Zagros. In G. I. Alsop, D. J. Blundell, & I. Davison (Eds.), *Salt tectonics* (Vol. 100, pp. 89–109). London: special publication of the Geological Society.
- Talebian, M., & Jackson, J. (2002). Offset on the Main Recent Fault of NW Iran and implications for the late Cenozoic tectonics of the Arabia-Eurasia collision zone. *Geophysical Journal International*, *150*, 422–439. <https://doi.org/10.1046/j.1365-246x.2002.01711.x>
- Talebian, M., & Jackson, J. (2004). A reappraisal of earthquake focal mechanisms and active shortening in the Zagros mountains of Iran. *Geophysical Journal International*, *156*, 506–526. <https://doi.org/10.1111/j.1365-246x.2004.02092.x>
- Tavakoli, F., Walpersdorf, A., Authemayou, C., Nankali, H. R., Hatzfeld, D., Tatar, M., et al. (2008). Distribution of the right-lateral strike-slip motion from the Main Recent Fault to the Kazerun Fault System (Zagros, Iran): Evidence from present-day GPS velocities. *Earth and Planetary Science Letters*, *275*, 342–347. <https://doi.org/10.1016/j.epsl.2008.08.030>
- Taymaz, T., Jackson, J. A., & McKenzie, D. (1991). Active tectonics of the north and central Aegean Sea. *Geophysics Journal International*, *106*, 403–490. <https://doi.org/10.1111/j.1365-246x.1991.tb03906.x>
- Vernant, P., Nilfouroushan, F., Hatzfeld, D., Abbassi, M., Vigny, C., Masson, F., et al. (2004). Contemporary crustal deformation and plate kinematics in Middle East constrained by GPS measurements in Iran and northern Iran. *Geophysical Journal International*, *157*, 381–398. <https://doi.org/10.1111/j.1365-246X.2004.02222.x>
- Walker, R. T., Andalibi, M. J., Gheitanchi, M. R., Jackson, J. A., Karegar, S., & Priestley, K. (2005). Seismological and field observations from the 1990 November 6 Furg (Hormozgan) earthquake: A rare case of surface rupture in the Zagros mountains of Iran. *Geophysical Journal International*, *163*, 567–579. <https://doi.org/10.1111/j.1365-246x.2005.02731.x>
- Walpersdorf, A., Hatzfeld, D., Nankali, H., Tavakoli, F., Nilfouroushan, F., Tatar, M., et al. (2006). Difference in the GPS deformation pattern of north and central Zagros (Iran). *Geophysical Journal International*, *167*, 1077–1088. <https://doi.org/10.1111/j.1365-246x.2006.03147.x>
- Yang, S., Li, J., & Wang, Q. (2008). The deformation pattern and fault rate in the Tianshan Mountains inferred from GPS observations. *Science in China Series D-Earth Sciences*, *51*, 1064–1080. <https://doi.org/10.1007/s11430-008-0090-8>
- Zarifi, Z., Nilfouroushan, F., & Raeesi, M. (2014). Crustal stress map of Iran: Insight from seismic and geodetic computations. *Pure and Applied Geophysics*, *171*, 1219–1236. <https://doi.org/10.1007/s00024-013-0711-9>